Carbohydrate Polymers 113 (2014) 525–531

Contents lists available at ScienceDirect

Carbohydrate Polymers

journal homepage: www.elsevier.com/locate/carbpol

# Catalytic reduction of *p*-nitrophenol by using platinum nanoparticles stabilised by guar gum

Sadanand Pandey*, Shivani B. Mishra

*Department of Applied Chemistry, University of Johannesburg, 37 Nind Street, Doornfontein, Johannesburg 2028, South Africa*

ARTICLE INFO

*Article history:*
Received 5 May 2014
Received in revised form 8 July 2014
Accepted 14 July 2014
Available online 28 July 2014

*Keywords:*
Biopolymer
Guar gum
Metal nanoparticle
Green method
Catalysis
*p*-Nitrophenol

ABSTRACT

We report a facile and green method to synthesise highly stable dispersions of platinum nanoparticles (PtNPs) with an average particle size of ~6 nm. Natural, nontoxic, eco-friendly biopolymer guar gum was utilised as both the reducing and capping agent precursor in aqueous medium. The PtNPs that had been stabilised by guar gum (GG-*s*-PtNPs) were characterised by UV–vis spectroscopy, XRD, TEM and XPS. GG-*s*-PtNPs performed better in terms of catalytic activity for the liquid phase reduction of *p*-nitrophenol (*p*-NP) compared to *p*-aminophenol (*p*-AP). The efficiency of the catalytic reduction of *p*-NP over GG-*s*-PtNPs was found to be 97% in a total time of 320 s at room temperature. The mechanisms of the synthesis and catalytic reduction of *p*-NP are also discussed. The synthesis approach presented here does not require stringent conditions or toxic agents and thus is a straightforward, rapid, efficient, and green approach to the fabrication of highly active catalysts.



## 1. Introduction

*Para*-nitrophenol (*p*-NP) is one of the hazardous and toxic pollutants, which is known to cause adverse health effects in living organisms. It is known to be anthropogenic, toxic and inhibitory in nature. *Para*-nitrophenols are widely used in the manufacture of pesticides, insecticides, fungicides, synthetic dyes, pharmaceuticals and to darken leather (Agency for Toxic Substances and Disease Registry (ATSDR), 1990). Human exposure to *p*-NP takes place by three pathways, namely inhalation, ingestion (eating, drinking) and dermal contact. The severity of health effects after exposure to *p*-NP depends on exposure dose, duration, pathways and individual characteristics such as gender, nutritional status, family traits, lifestyle, and state of health. Short-term exposure of *p*-NP by the pathways of inhalation or ingestion causes symptoms such as headaches, drowsiness, nausea, and cyanosis. Contact with eyes results in irritation (U.S. Department of Health and Human Services (USDHHS), 1993). *Para*-nitrophenol is one of the most toxic derivatives of the parathion insecticide and is carcinogenic, hazardous, mutagenic and toxic (cytotoxic and embryo-toxic) to mammals (Banik, Prakash, & Upadhyay, 2008).

*Para*-Nitrophenol is known to be highly soluble and stable in water bodies such as freshwater, marine environments and in industrial wastewaters. Due to its solubility, traditional water purification methods to remove *p*-NP from contaminated wastewater are not effective. Scientists have therefore developed many techniques for *p*-NP removal which include adsorption, microwave-assisted catalytic oxidation, microbial degradation, photocatalytic degradation, electro-Fenton method, electrocoagulation, and electrochemical treatment (Marais & Nyokong, 2008; O'Connor & Young, 1989; Dieckmannand & Gray, 1996; Bo, Zhang, Quan, & Zhao, 2008; Modirshahla, Behnajady, & Mohammadi-Aghdam, 2008; Canizares, Sez, Lobato, & Rodrigo, 2004). However, all these techniques are energy-consuming and involve the use of organic solvents. Therefore, in the present scenario, it is very important to develop and employ aqueous phase conversion of *p*-NP to *p*-AP under mild conditions. *Para*-nitrophenol is converted to *p*-AP by catalytic reduction method. The reduction product (*p*-AP) obtained from the catalytic reduction of *p*-NP is effective in many useful applications such as analgesic and antipyretic drugs, photographic developer, corrosion inhibitor, anticorrosion lubricant, etc. (Shin, Choi, Park, Jang, & Kim, 2009).

The use of many noble metal–alloy nanoparticles for water treatment has been reported extensively in the literature, but reports on applications of precious-metal nanoparticles are quite limited in the literature. Precious-metal nanoparticles have been attracting a lot of interest recently because of their significant properties of high activity (Pandey, Goswami, & Nanda, 2012; Pandey, Goswami, & Nanda, 2013a), excellent efficiency, and higher Fermi potential which result in lowering of the reduction potential value, and hence metal nanoparticles act as active catalysts

* Corresponding author. Tel.: +27 11 5596163; fax: +27 11 5596644.
*E-mail addresses:* spandey.uj@gmail.com, sadanand.au@gmail.com, spandey@uj.ac.za (S. Pandey).

http://dx.doi.org/10.1016/j.carbpol.2014.07.047
0144-8617/

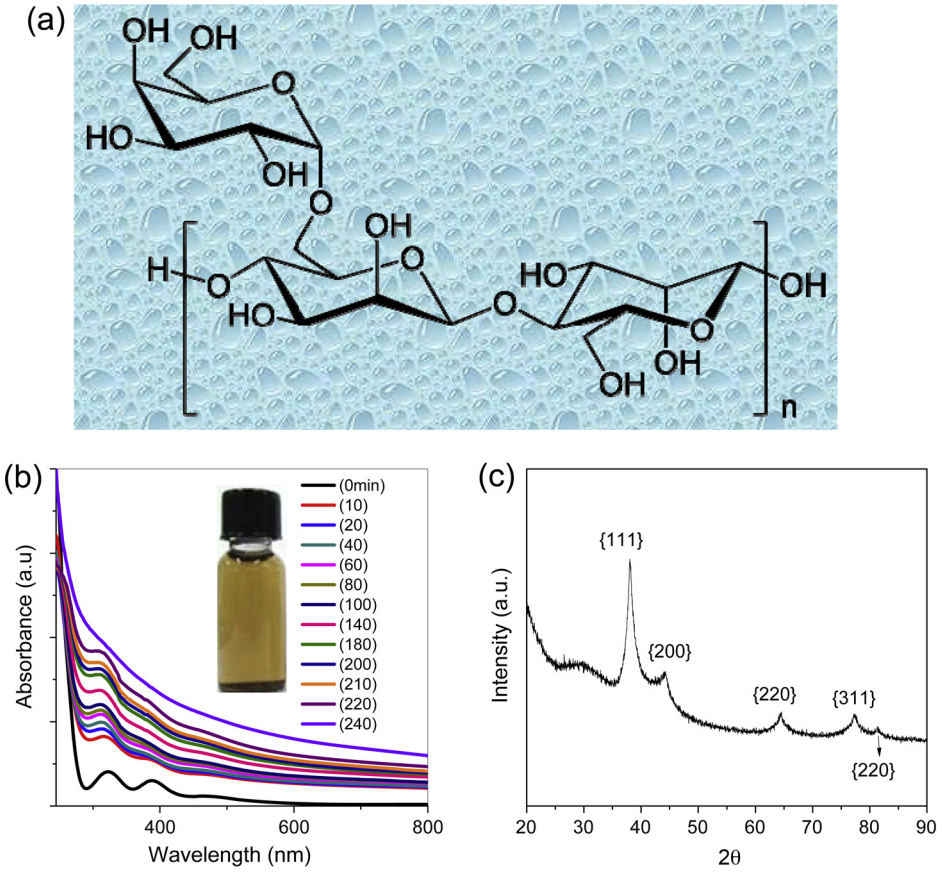


**Fig. 1.** (a) Structure of guar gum; (b) spectral changes of the GG-*s*-PtNPs at various time intervals (10 min to 240 min) recorded using UV–vis spectroscopy (GG-*s*-PtNPs solution is shown in the inset); and (c) XRD pattern of GG-*s*-PtNPs.

for many electron-transfer reactions (Ismail et al., 2011; Ismail & Bahnemann, 2011; Ghosh, Mandal, Kundu, Nath, & Pal, 2004). There are various methods for the synthesis of precious-metal nanoparticles such as electrochemical synthesis, radiation, chemical reduction, photochemical reduction, etc. However, the focus in this article is on the green method for the synthesis of precious-metal nanoparticles (PtNPs) by using guar gum (GG). Guar gum is a high-molecular-weight polysaccharide that is abundantly available in nature; its backbone is a linear chain of β-D(1 → 4) mannopyranosyl units with 1 → 6 linked α-D-galactopyranosyl units as side-chains. The structure of GG is shown in Fig. 1(a).

The catalytic properties of precious-metal nanoparticle catalysts depend on the size and distribution of the nanoparticles and on the interactions between the metal nanoparticles and the nature of the support (Tian, Zhang, Tong, & Chen, 2008; Hervés et al., 2012; Sen, Maity, & Islam, 2013; Xu et al., 2014). Catalytic reduction of *p*-NP in the presence of $NaBH_4$ has already been performed using Au nanoparticles deposited on poly(methyl methacrylate) (PMMA) (Kuroda, Ishida, & Haruta, 2009), Au/polypyrrole nanotubes (Qiu et al., 2012), Pd/$Al_2O_3$ (Arora, Kapoor, & Singla, 2010), Pd/polypyrrole nanocapsules (Hwang, Sang-Ho, Hoon, Kim, & Choi, 2008), and Ag/SBA-15 (Zhang et al., 2012). Dubey et al. (2014) fabricated graphene–carbon sphere hybrid aerogel decorated with silver nanoparticles (G/AgCS) for the catalytic reduction of *p*-NP in the presence of $NaBH_4$, while Jan, Chuang, Chen, and Teng (2011) used layer-by-layer polypeptide assemblies to mediate the synthesis of Au/mesoporous silica nanotubes with the apparent rate constant of $3 \times 10^{-4}$ and $8 \times 10^{-4}$ $s^{-1}$ for Au/SNTs obtained from $(Lys340/Glu125)_5$ and $(Lys340/PLT)_5$ coated membranes.

Herein, we demonstrate a simple, environmentally friendly, and cost-effective method for preparing highly stable dispersions of nanosized platinum particles derived from a natural biopolymer. The reaction is carried out in an aqueous medium solution and guar gum is used as both reducing and capping agent to prevent the aggregation of platinum nanoparticles. No other chemical is added to avoid any adverse effect on the performance of the products. Additionally, these GG-*s*-PtNPs were successfully used in the catalytic reduction of *p*-NP as a model reaction. To the best of our knowledge, this is the first report on spherical PtNPs formed with guar gum (GG); details of the synthesis and characterisation of the novel GG-*s*-PtNPs are provided, as are the results of the investigation into their catalytic activities.

## 2. Experimental

### 2.1. Materials

Potassium tetrachloroplatinate(II), ($K_2$ $PtCl_4$ 98%) was purchased from Sigma-Aldrich (USA) and used without further purification. Guar gum (GG), *p*-nitrophenol (*p*-NP) and sodium hydroxide (NaOH) were purchased from Merck (South Africa). All aqueous solutions were made up using ultrahigh deionised (DI) water purified using a Milli-Q Plus system (Millipore Co.).

### 2.2. Preparation of PtNPs stabilised with guar gum (GG-s-PtNPs)

All glassware used during synthesis was cleaned in a bath of freshly prepared aqua regia solution (HCl: $HNO_3$, 3:1), and rinsed thoroughly with deionised water prior to use. For the synthesis of GG-*s*-PtNPs, a stock solution of 2.5 mM was prepared by adding $K_2PtCl_4$ (0.0415 g) in DI water. Thereafter the $K_2PtCl_4$ solution was mixed with GG solution followed by the addition of a few drops of

very dilute solution of NaOH (0.001 M) at room temperature until reaching pH 8. The total volume of DI water was kept at 40 mL. The solutions were then stirred gently at the desired temperature (70 °C) for 240 min, during which time the colourless solution was converted to the characteristic light brown solution indicating the formation of GG-*s*-PtNPs. It was observed that the aqueous solution of GG-*s*-PtNPs was stable for more than 9 months.

### 2.3. Characterisation of synthesised GG-s-PtNPs

The GG-*s*-PtNPs were characterised by using X-ray diffraction (XRD) using a Bruker D8 Advance powder diffractometer operating in the reflection mode with Cu*K*α radiation. The size of the NPs was determined by means of transmission electron microscopy (TEM) using a Tecnai T20 microscope operating at 200 kV equipped with an EDS (energy dispersive spectrum) detector. X-ray photoelectron spectroscopy (XPS) analysis was carried out by using a Kratos Axis Ultra DLD spectrometer to confirm the composition of the surface layer of nanoparticle to be metallic platinum. Spectroscopy was carried out with a Shimadzu UV-1800 spectrophotometer to confirm the formation of PtNPs.

### 2.4. Catalytic reduction of p-nitrophenol (p-NP)

A standard catalytic test reaction was carried out in a quartz cuvette. For a catalytic reduction of *p*-nitrophenol, 100 μL of *p*-NP (1 mM) and 1 mL $NaBH_4$ (0.1 M) were added to a quartz cuvette containing 3 mL of deionised water. Thereafter 50 μL of an aqueous solution containing GG-*s*-PtNPs (2.5 mM) was injected into the cuvette to start the reaction. The intensity of the absorption peak at 400 nm in the UV–vis spectrophotometer was used to monitor the process of the conversion of *p*-nitrophenol (*p*-NP) to *p*-aminophenol (*p*-AP). The percentage catalytic conversion efficiency of *p*-NP to *p*-AP in the reaction process was calculated using the following equation:

$$\% = \frac{C_0 - C_n}{C_0} \times 100 \quad (1)$$

where $C_n$ is the concentration of *p*-AP measured at time *t*, $C_0$ is the initial concentration of *p*-AP measured at time zero.

## 3. Results and discussion

### 3.1. UV–vis spectroscopy characterisation

One of the most simple, easy and convenient techniques for characterisation of GG-*s*-PtNPs was UV–vis spectroscopy. Due to the ligand-to-metal charge transfer transition of the $PtCl_4^{2-}$, it exhibited a peak at 320 nm in its UV–vis spectrum as shown in Fig. 1(b). It was observed that with increasing time, the colour of the solution gradually changed from colourless to light brown. The peak at 320 nm disappeared after 4 h of the reaction as shown in Fig. 1(b), indicating that the Pt (II) was completely reduced to Pt (0). The PtNPs showed absorption in all ranges of the UV–vis spectrum and the absorption increased with the decrease in wavelength.

### 3.2. XRD

The synthesis of platinum nanoparticles can be evaluated with XRD methods. The XRD patterns of GG and PtNPs are compared. As we already know, the XRD of GG shows the amorphous nature of the material (Pandey, Goswami, & Nanda, 2013b), while the XRD profile of PtNPs presented in Fig. 1(c) exhibits characteristic peaks at scattering angles (2$\theta$) of 38.06, 44.22, 64.48, 77.32 and 81.2 corresponding with scattering from the (1 1 1), (2 0 0), (2 2 0), (3 1 1) and (2 2 2) planes, respectively. These are consistent with the face-centred cubic (fcc) structure of platinum, and can be assigned to JCPDS Card 04-0802, thus demonstrating the presence of crystalline Pt (Shah, 2012). The most intense lattice plane reflection (1 1 1) from the Pt nanoparticles was used to calculate the average size of Pt nanocrystallites on the basis of the width of the reflection according to the Debye–Scherrer equation:

$$\tau = \frac{K\lambda}{\beta \cos\theta} \quad (2)$$

where $\tau$ is the mean size of the ordered (crystalline) domains, which may be smaller than or equal to the grain size, $K$ is a dimensionless shape factor, with a value close to unity, $\lambda$ is the X-ray wavelength, $\beta$ is the line broadening at half the maximum intensity (FWHM); $\theta$ is the Bragg angle.

Based on the above Debye–Scherrer equation, the crystallite size of PtNPs was estimated to be about 7 nm, which is in good agreement with TEM results obtained.

### 3.3. Transmission electron microscopy (TEM)

In order to measure the shape and size of NPs, transmission electron microscopy (TEM) grids were prepared by placing 500 μL of the PtNP solution on a carbon-coated copper grid and subsequent drying under a table lamp at room temperature. TEM was performed using a Tecnai T20 microscope operating at 200 kV equipped with an EDS (energy dispersive spectrum) detector. TEM images were taken from different locations of the grid and with different magnifications. Approximately 355 particles were counted and measured for size distribution using ImageJ software. Fig. 2(a) shows a typical TEM image of Pt nanoparticles in colloidal solutions prepared using hexachloroplatinic acid. The spherical shape was confirmed with the high-resolution bright field TEM images of PtNPs (Fig. 2(b)). It was shown that the average size of Pt nanoparticles depends on the concentration of hexachloroplatinic acid. If the concentration of hexachloroplatinic acid is 2.5 mM then the average size of Pt nanoparticles is 6.2 nm as shown in Fig. 2(a). The 5 mM of concentration of hexachloroplatinic acid gives average size of 9 nm of Pt nanoparticles (figure not shown). The average size of Pt nanoparticles in colloidal solution increases from 6.2 nm to 9 nm with increasing precursor concentration. The lattice fringes in processed high-resolution TEM images (Fig. 2(b)) show that the GG-*s*-PtNPs are single crystals, and also reveal that the particles have a lattice *d*-spacing of 0.223 nm, 0.137 nm, 0.111 nm and 0.116 nm and their indices (*h k l*) are assigned to the (1 1 1), (2 2 0), (2 2 2) and (3 1 1) planes of Pt, respectively, corresponding to JCPDS Card 04-0802, and indicating a face-centred cubic (fcc) crystalline structure. EDX shows the presence of % Pt content is more than C and O (figure not shown). Fig. 2(c) shows the particle size distribution histograms of PtNPs formed after 240 min. The size distribution is almost Gaussian. The mean particle size is ~6.2 nm, calculated from 355 nanoparticles. Samples are characterised by particles with a narrow particle-size distribution width with typical standard deviations (SDs) of 13%. Therefore, the synthesised PtNPs are almost monodisperse.

The mechanism for growth of monodisperse colloidal particles, i.e., the kinetics of "growth by diffusion", is discussed by Reiss (1951). The spherical shaped platinum nanoparticles are formed in the presence of the biopolymer (guar gum), which acts as a capping material. The presence of the guar gum in the solution of colloids is now believed to have mainly two functions: the first is to maintain the growth of small particle sizes; and its second function is to prevent individual colloidal particles from coalescing with each other, thus giving the colloids a higher degree of monodispersity. The Comparison of size/shape of PtNPs created from GG to other polysaccharides elucidated that

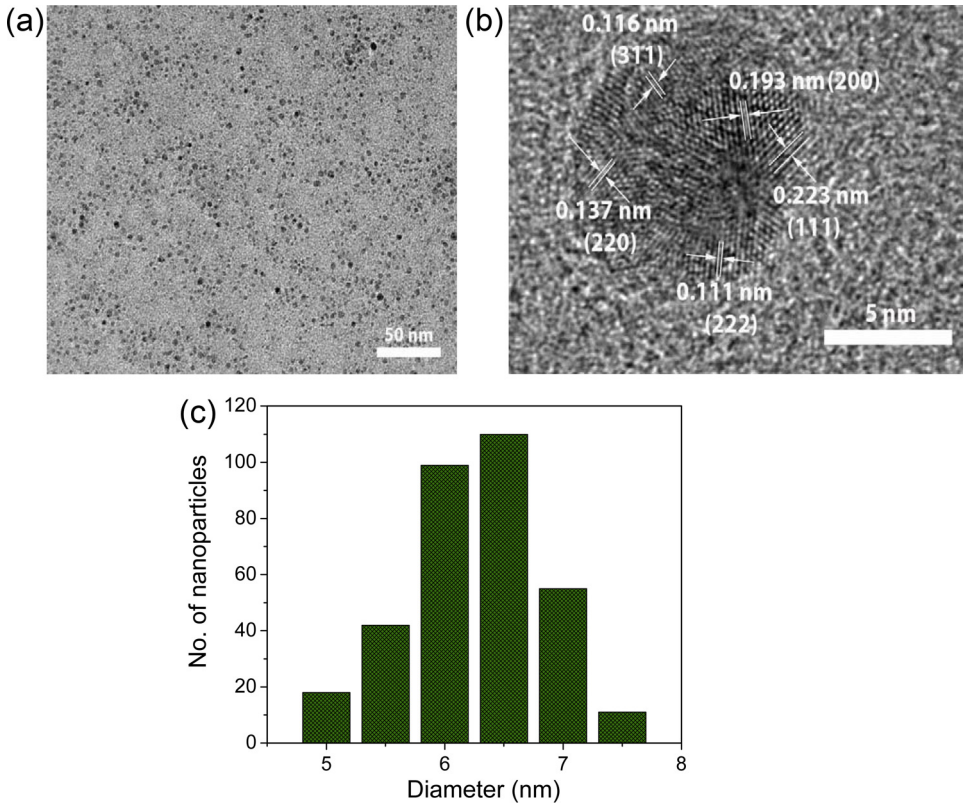


**Fig. 2.** (a) A typical TEM image of Pt nanoparticles in colloidal solutions prepared using hexachloroplatinic acid; (b) lattice fringes in processed HRTEM images confirming face-centred cubic structure; and (c) particle size distribution histograms of PtNPs formed after 240 min.

the polysaccharides is the most efficient green method in PtNPs synthesis. There are very limited literatures for synthesis of PtNPs by polysaccharides. The rate of PtNPs synthesis by polysaccharide was higher. In addition, this method showed easy, energy saving, cost-effective, rapid synthesis, high productivity and small or no aggregation of synthesised PtNPs with excellent stability. The size/shape and other parameters of PtNPs synthesis by different polysaccharides reported by researchers (Adlim, Bakar, Liew, & Ismail, 2004; Vinod, Saravanan, Sreedhar, Devi, & Sashidhar, 2011; Liu, Sutton, & Roberts, 2007; Li, Zhang, Huang, Ye, & Lin, 2014; Benaissi, Johnson, Walsh, & Thielemans, 2010; He, Kunitake, & Nakao, 2003; Tongsakul, Nishimura, Thammacharoen, Ekgasit, & Ebitani, 2012; Coccia, Tonucci, Bosco, Bressan, & d'Alessandro, 2012) were compared in Table 1.

The formation of PtNPs was further confirmed by XPS (figure not provided). For XPS, a droplet of the PtNP suspension was drop-cast on a Si substrate (cleaned in HF–water solution prior to use) and left to dry, before recording the spectrum. The XPS spectrum shows two well-defined peaks with binding energies of 71.3 eV and 74.5 eV, which were attributed to the Pt 4f7/2 and Pt 4f5/2 doublet

**Table 1**
Comparison of size/shape of PtNPs created from GG to other polysaccharides.

| Polysaccharide | Reducer | Stabilizer | Stability | Reaction time | Dispersion of metal particles | Average size/shape | References |
|---|---|---|---|---|---|---|---|
| Guar gum | GG | GG | >9 months | 240 min | Highly dispersed | 6.2 nm. Spherical | This work |
| Chitosan | Methanol<br>$NaBH_4$<br>Hydrazine | Chitosan | – | 33 min | Dispersed<br>Dispersed<br>Aggregated | 1–2 nm<br><3 nm<br>> 16.91 | Adlim et al. (2004) |
| Gum kondagogu (Cochlospermum gossypium) GK | GK | GK | >6 months | – | Dispersed | 2.4 | Vinod et al. (2011) |
| Sodium carboxymethyl cellulose (CMC) | $NaBH_4$ | CMC | 9 months | 30 min | Dispersed | 3.9 nm (spherical and faceted particles) | Liu et al. (2007) |
| Graphene Nanosheets–cyclodextrin GNs-CD | $NaBH_4$ | GNs-CD | – | 2880 min | Dispersed | 3–5 nm (hydrangea-like nanoclusters) | Li et al. (2014) |
| Cellulose nanofibrils from cotton | Cellulose nanofibrils | – | – | 1440 min | – | 5–30 nm (spherical) | Benaissi et al. (2010) |
| Cellulose fibres | $NaBH_4$ | Cellulose fibers | | – | Dispersed | 5.7 | He et al. (2003) |
| Hydrotalcite supported-Pt NPs catalyst by using soluble starch | Starch | Starch | | 20 min | Dispersed | 2.1 | Tongsakul et al. (2012) |
| Lignin | Lignin | Lignin | 1 month | 180 min | Aggregate | 6–8 nm (irregular) | Coccia et al. (2012) |

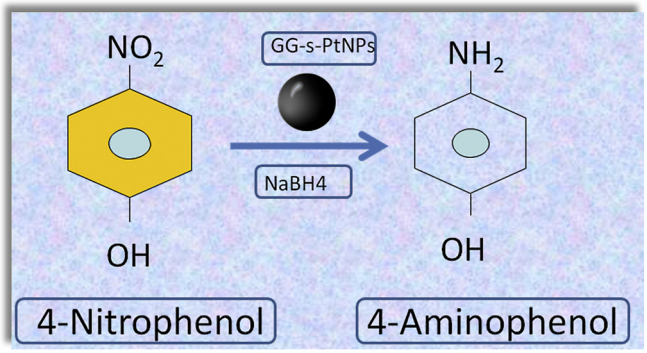


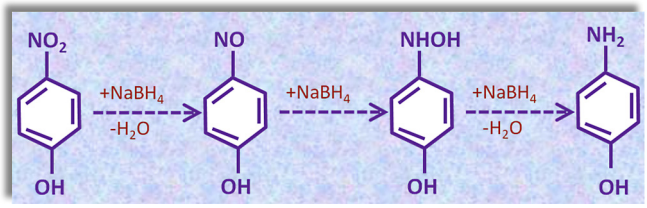


**Scheme 1.** Representation of the overall reaction process for converting *p*-NP to *p*-AP by $NaBH_4$ in the presence of GG-*s*-PtNPs as a catalysts

in Pt(0), respectively (Moulder, Stickle, Sobol, & Bomben, 1992). This demonstration reveals the formation of PtNPs.

### 3.4. Reduction of p-NP to p-AP

The catalytic activities of the GG-*s*-PtNP catalysts were investigated using the reduction of *p*-NP to *p*-AP in the presence of $NaBH_4$ as a model reaction (Scheme 1). A strong absorbance peak was found for *p*-NP at 317 nm that shifted to 400 nm in the presence of $NaBH_4$ due to the deprotonation of 4-NP (p*K*a of 4-NP = 7.16) (Pradhan, Pal, & Pal, 2002). The pH of the solution was increased to pH 11 upon addition of $NaBH_4$. After adding $NaBH_4$ into the aqueous solution of *p*-NP, the colour of the solution also changed from light yellow to intense yellow due to the formation of *p*-nitrophenolate ion. However, no reduction was observed, even after a period of 2 days to 3 days in the presence of $NaBH_4$ or GG. Metal nanoparticles, such as silver, copper, gold, and platinum, are known to expedite electron transfer from donors (in this case $BH_4^-$) to acceptors (in this case *p*-NP) (Gangula, Podila, Karanam, Janardhana, & Rao, 2011). Thus, the colour of the 4-nitrophenolate ions faded with time after the addition of catalyst GG-*s*-PtNPs. The progress of the reaction was monitored by UV–vis absorbance spectroscopy and visually by the disappearance of the yellow colour of *p*-NP.

The characteristic peak of *p*-NP at 400 nm decreased, while at 300 nm a new peak appeared which was assigned to *p*-AP (Fig. 3(a) and (c)). The reaction was completed within 360 s at 25 °C. This illustrates the spontaneous activity and the high speed of the GG-*s*-PtNPs catalytic activity and also its high selectivity for *p*-AP yield (Fig. 3(a) and (c)).

The probable reaction steps for catalytic decomposition *p*-NP to *p*-AP are as follows:

It is known that $NaBH_4$ acts as a hydrogen source that liberates hydrogen gas by hydrolysis at room temperature, and this process can be catalytically accelerated by metals (Rakap & Özkar, 2012). It has been suggested that the catalytic decomposition of $BH_4^-$ by PtNPs produces H-Pt and $PtBH_3^-$ as reactive intermediates (Eq. (3)) (Holbrook & Twist, 1971):

$$2Pt + BH_4^- \leftrightarrow Pt - BH_3^- + Pt - H \quad (3)$$

These species are believed to be responsible for the reduction of *p*-NP to *p*-AP (Eqs. (4) and (5); stoichiometrically, a six-electron reduction is required to transform *p*-NP to *p*-AP).

$$6H - Pt + p - NP \rightarrow p - AP + 6Pt + 6H^+ \quad (4)$$

$$6Pt - BH_3^- + p - NP \rightarrow p - AP + 6Pt + 6BH_3 \quad (5)$$

For the evaluation of the catalytic rate, the pseudo-first-order kinetics w.r.t. *p*-NP is a reasonable assumption (Fattah & Wixtrom, 2014; Chi et al., 2012). In this regard, the ratio of absorbance $A_t$ of *p*-NP at time *t* to its value $A_0$ measured at $t = 0$ must be equal to the concentration ratio $C_t/C_0$ of *p*-NP.

The kinetic equation for the reduction can be written as:

$$\frac{dC_t}{dt} = -K_{ap}C_t \quad \text{or} \quad \ln\left(\frac{C_t}{C_0}\right) \quad \text{or} \quad \ln\left(\frac{A_t}{A_0}\right) = -K_{app} \quad (6)$$

where $C_t$ is the concentration of *p*-NP at time *t*, $K_{app}$ is the apparent rate constant, which can be obtained from the decrease of the peak intensity at 400 nm over time.

Fig. 3(b) and (d) show a linear correlation between $\ln(A_t/A_0)$ ($A_t$: absorbance at fixed intervals, $A_0$: absorbance at the initial stage) and the reaction time at 25 °C, indicating that the reaction follows pseudo-first-order kinetics. The pseudo-first-order rate constant ($k$) at 25 °C was calculated from the slope to be $8.3 \times 10^{-3}$ $s^{-1}$ and $7 \times 10^{-3}$ $s^{-1}$ in the case of PtNPs (6 nm and 9 nm, respectively), which was the highest value among the other reported nanocatalysts (Chi et al., 2012; Xue, Lu, Bian, Lei, & Wang, 2012; Huang et al., 2012; Fattah & Wixtrom, 2014; Sen et al., 2013; Esumi, Isono, & Yoshimura, 2004). The apparent rate constants of this catalytic reaction in the presence of different metal catalysts are presented in Table 2 as measured from the plot of $\ln(A_t/A_0)$ vs. time. The comparison results were shown in Table 2. It clearly displayed that

**Table 2**
Comparison of apparent rate constants of catalytic reaction in the presence of different metal catalysts.

| Catalyst | Type | Target compound | Conc. (M) | Catalyst dose | Degradation rate ($s^{-1}$) | References |
|---|---|---|---|---|---|---|
| GG-*s*-PtNPs | Spherical | *p*-NP | $0.1 \times 10^{-3}$ | 5 mM (50 μL) | $7 \times 10^{-3}$ | This work |
| $Fe_3O_4$@$SiO_2$–Ag | Spherical | *p*-NP | $0.12 \times 10^{-3}$ | 1 g | $7.67 \times 10^{-3}$ | Chi et al. (2012) |
| Pd/polypyrrole | Nanocapsule | *p*-NP | $1.07 \times 10^{-4}$ | 0.006 mg $mL^{-1}$ | $8.8 \times 10^{-3}$ | Xue et al. (2012) |
| CuNPs | Dumbbell-like | *p*-NP | $3.3 \times 10^{-3}$ | 0.096 mg $mL^{-1}$ | $8.3 \times 10^{-3}$ | Huang et al. (2012) |
| AuNPs@MWCNT | – | *p*-NP | $6.3 \times 10^{-5}$ | – | $1.10 \times 10^{-4}$ | Abdel-Fattah and Wixtrom (2014) |
| AuNPs–glucan bioconjugates | Spherical ~8 nm | *p*-NP | – | – | $3.3 \times 10^{-4}$ | Sen et al. (2013) |
| PPI Dendrimer (G4)–AgNC | Spherical | *p*-NP | 0.3 $cm^3$ of 2 mmol $dm^{-3}$ | 20 (mmol $dm^{-3}$) | $4.13 \times 10^{-4}$ | Esumi et al. (2004) |
| PAMAM dendrimer(G4)–AgNC | spherical | *p*-NP | 0.3 $cm^3$ of 2 mmol $dm^{-3}$ | 10 (mmol $dm^{-3}$) | $5.9 \times 10^{-4}$ | Esumi et al. (2004) |
| PAMAM dendrimer(G4)–PdNC | Spherical | *p*-NP | 0.3 $cm^3$ of 2 mmol $dm^{-3}$ | 10 (mmol $dm^{-3}$) | $17.9 \times 10^{-4}$ | Esumi et al. (2004) |
| PAMAM dendrimer(G4)–PtNC | Spherical 1.2—1.6 nm | *p*-NP | 0.3 $cm^3$ of 2 mmol $dm^{-3}$ | 10 (mmol $dm^{-3}$) | $26.2 \times 10^{-4}$ | Esumi et al. (2004) |
| PPI Dendrimer (G4)–PtNC | Spherical | *p*-NP | 0.3 $cm^3$ of 2 mmol $dm^{-3}$ | 20 (mmol $dm^{-3}$) | $33.9 \times 10^{-4}$ | Esumi et al. (2004) |

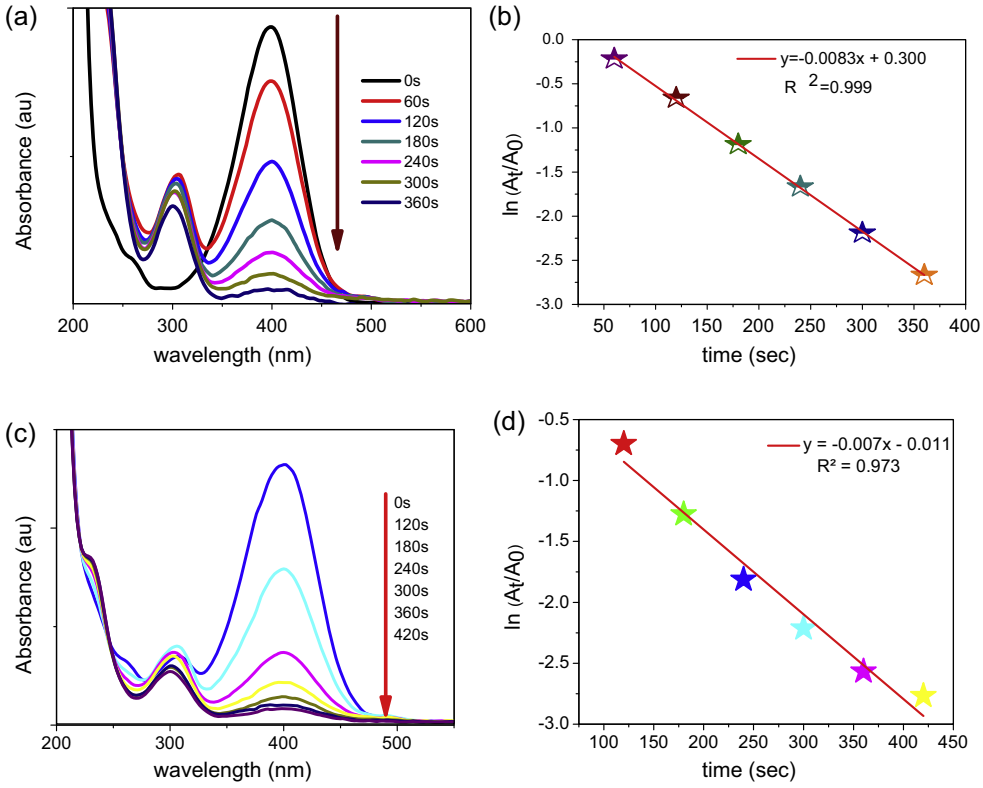


**Fig. 3.** (a) to (d) Successive UV–vis spectra of the reduction of *p*-nitrophenol by spherical PtNPs (6 nm) and (9 nm); (c) and (d) plot of $A_t/A_0$ vs. time for two different PtNPs (6 nm) and (9 nm).

**Table 3**
Conversion (%) for the reduction of *p*-nitrophenol to *p*-aminophenol by PtNPs (5 nm) and PtNPs (9 nm) catalysts.

| Time (s) | Conversion (%) | |
|---|---|---|
| | Pt NPs (6 nm) | Pt NPs (9 nm) |
| 120 | 48.3 | 40 |
| 180 | 69.5 | 72 |
| 240 | 81.1 | 83.6 |
| 300 | 88.8 | 89 |
| 360 | 97 | 92.3 |
| 420 | – | 93.7 |

GG-*s*-PtNPs possessed higher catalytic activity than other nanocatalysts.

The efficiency of the catalytic reduction of *p*-NP over GG-*s*-PtNPs was found to be 97% and 92.3% after 320 s in the case of PtNPs (6 nm and 9 nm, respectively) (Table 3). The excellent performance of the Pt catalyst can be explained based on the morphology, particle size and distribution, since Pt nanoparticles were significantly smaller in size (6 nm) having a large surface area and being highly monodisperse. This results in high efficiency of PtNPs for the reduction of *p*-NP.

## 4. Conclusion

We reported a facile and green method to synthesise highly stable dispersions of platinum nanoparticles (PtNPs) with an average particle size of ~6 nm. Natural, nontoxic, eco-friendly biopolymer guar gum was utilised as both reducing and capping agent precursor in aqueous medium. In addition, the as-prepared GG-*s*-PtNPs possessed excellent colloidal stability in aqueous solution and exhibited superior catalytic activity towards the reduction of *p*-nitrophenol (*p*-NP).

## Acknowledgements

The author is grateful for the generous financial support received from the National Research Foundation (NRF) and for instrumentation and laboratory facilities made available by the University of Johannesburg, Johannesburg, South Africa.

## References

Abdel-Fattah, T. M., & Wixtrom, A. (2014). Catalytic reduction of 4-nitrophenol using gold nanoparticles supported on carbon nanotubes. *ECS Journal of Solid State Science and Technology*, *3*(4), M18–M20.

Adlim, M., Bakar, M. A., Liew, K. Y., & Ismail, J. (2004). Synthesis of chitosan-stabilized platinum and palladium nanoparticles and their hydrogenation activity. *Journal of Molecular Catalysis A: Chemical*, *212*, 141–149.

Agency for Toxic Substances and Disease Registry (ATSDR). (1990). *Toxicological profile for nitrophenols (draft)*. Atlanta, GA: Public Health Service, U.S. Department of Health and Human Services.

Arora, S., Kapoor, P., & Singla, M. L. (2010). Catalytic studies of palladium nanoparticles immobilized on alumina synthesized by a simple physical precipitation method. *Reaction Kinetics, Mechanisms, and Catalysis*, *99*, 157–165.

Banik, R. M., Prakash, M. R., & Upadhyay, S. N. (2008). Microbial biosensor based on whole cell of *Pseudomonas* sp. for online measurement of *p*-nitrophenol. *Sensors and Actuators B: Chemical*, *131*, 295–300.

Benaissi, K., Johnson, L., Walsh, D. A., & Thielemans, W. (2010). Synthesis of platinum nanoparticles using cellulosic reducing agents. *Green Chemistry*, *12*, 220–222.

Bo, L. L., Zhang, Y. B., Quan, X., & Zhao, B. (2008). Microwave assisted catalytic oxidation of *p*-nitrophenol in aqueous solution using carbon-supported copper catalyst. *Journal of Hazardous materials*, *153*, 1201–1206.

Canizares, P., Sez, C., Lobato, J., & Rodrigo, M. A. (2004). Electrochemical treatment of 4-nitrophenol-containing aqueous wastes using boron-doped diamond anodes. *Industrial & Engineering Chemistry Research*, *43*, 1944–1951.

Chi, Y., Yuan, Q., Li, Y., Tu, J., Zhao, L., Li, N., & Li, X. (2012). Synthesis of $Fe_3O_4$@$SiO_2$–Ag magnetic nanocomposite based on small-sized and highly dispersed silver nanoparticles for catalytic reduction of 4-nitrophenol. *Journal of Colloid and Interface Science*, *383*, 96–102.

Coccia, F., Tonucci, L., Bosco, D., Bressan, M., & d'Alessandro, N. (2012). One-pot synthesis of lignin-stabilised platinum and palladium nanoparticles and their catalytic behaviour in oxidation and reduction reactions. *Green Chemistry*, *14*, 1073–1078.

Dieckmannand, M. S., & Gray, K. A. (1996). A comparison of the degradation of 4-nitrophenol via direct and sensitized photocatalysis in $TiO_2$ slurries. *Water Research*, *30*, 1169–1183.

Dubey, S. P., Dwivedi, A. D., Kim, I.-C., Sillanpaa, M., Kwon, Y.-N., & Lee, C. (2014). Synthesis of graphene–carbon sphere hybrid aerogel with silver nanoparticles and its catalytic and adsorption applications. *Chemical Engineering Journal*, *244*, 160–167.

Gangula, A., Podila, R., Karanam, L., Janardhana, C., & Rao, A. M. (2011). Catalytic reduction of 4-nitrophenol using biogenic gold and silver nanoparticles derived from *Breynia rhamnoides*. *Langmuir*, *27*, 15268–15274.

Esumi, K., Isono, R., & Yoshimura, T. (2004). Preparation of PAMAM- and PPI-metal (silver, platinum, and palladium) nanocomposites and their catalytic activities for reduction of 4-nitrophenol. *Langmuir*, *20*, 237–243.

Ghosh, S. K., Mandal, M., Kundu, S., Nath, S., & Pal, T. (2004). Bimetallic Pt–Ni nanoparticles can catalyze reduction of aromatic nitro compounds by sodium borohydride in aqueous solution. *Applied Catalysis A: General*, *268*, 61–66.

He, J., Kunitake, T., & Nakao, A. (2003). Facile in situ synthesis of noble metal nanoparticles in porous cellulose fibers. *Chemistry of Materials*, *15*, 4401–4406.

Hervés, P., Pérez-Lorenzo, M., Liz-Mardân, L. M., Dzubiella, J., Lu, Y., & Ballauff, M. (2012). Catalysis by metallic nanoparticles in aqueous solution: Model reactions. *Chemical Society Reviews*, *41*, 5577–5587.

Holbrook, K., & Twist, P. (1971). Hydrolysis of the borohydride ion catalysed by metal–boron alloys. *J. Chem. Soc. A: Inorg. Phys. Theor.*, 890–894.

Huang, X. Q., Li, Y. J., Zhou, H. L., Zhong, X., Duan, X. F., & Huang, Y. (2012). Simplifying the creation of dumbbell-like Cu–Ag nanostructures and their enhanced catalytic activity. *Chemistry—A European Journal*, *18*, 9505–9510.

Hwang, C., Sang-Ho, K., Hoon, O. J., Kim, M., & Choi, S. (2008). Reduction of aromatic nitro compounds on Pd colloids prepared by γ-irradiation. *Journal of Industrial and Engineering Chemistry*, *14*, 864–868.

Ismail, A. A., & Bahnemann, D. W. (2011). One-step synthesis of mesoporous platinum/titania nanocomposites as photocatalyst with enhanced photocatalytic activity for methanol oxidation. *Green Chemistry*, *13*, 428–435.

Ismail, A. A., Bahnemann, D. W., Rathouskýí, J., Yarovyi, V., & Wark, M. (2011). Multilayered ordered mesoporous platinum/titania composite films: Does the photocatalytic activity benefit from the film thickness. *Journal of Materials Chemistry*, *21*, 7802–7810.

Jan, J.-S., Chuang, T.-H., Chen, P.-J., & Teng, H. (2011). Layer-by-layer polypeptide macromolecular assemblies-mediated synthesis of mesoporous silica and gold nanoparticle/mesoporous silica tubular nanostructures. *Langmuir*, *27*, 2834–2843.

Kuroda, K., Ishida, T., & Haruta, M. (2009). Reduction of 4-nitrophenol to 4-aminophenol over Au nanoparticles deposited on PMMA. *Journal of Molecular Catalysis A: Chemical*, *298*, 7–11.

Li, Z., Zhang, L., Huang, X., Ye, L., & Lin, S. (2014). Shape-controlled synthesis of Pt nanoparticles via integration of graphene and β-cyclodextrin and using as a noval electrocatalyst for methanol oxidation. *Electrochimica Acta*, *121*, 215–222.

Liu, J., Sutton, J., & Roberts, C. B. (2007). Synthesis and extraction of monodisperse sodium carboxymethylcellulose-stabilized platinum nanoparticles for the self-assembly of ordered arrays. *Journal of Physical Chemistry C*, *111*, 11566–11576.

Marais, E., & Nyokong, T. (2008). Adsorption of 4-nitrophenol onto Amberlite IRA-900 modified with metallophthalocyanines. *Journal of Hazardous materials*, *152*, 293–301.

Modirshahla, N., Behnajady, M. A., & Mohammadi-Aghdam, S. (2008). Investigation of the effect of different electrodes and their connections on the removal efficiency of 4-nitrophenol from aqueous solution by electrocoagulation. *Journal of Hazardous materials*, *154*, 778–786.

Moulder, J. F., Stickle, W. F., Sobol, P. E., & Bomben, K. D. (1992). In J. Chastain (Ed.), *Handbook of X-ray photoelectron spectroscopy*. Berlin: Perkin–Elmer Corporation (Physical Electronics).

O'Connor, A. O., & Young, L. Y. (1989). Toxicity and anaerobic biodegradability of substituted phenols under methanogenic conditions. *Environmental Toxicology and Chemistry*, *8*, 853–862.

Pandey, S., Goswami, G. K., & Nanda, K. K. (2012). Green synthesis of biopolymer–silver nanoparticle nanocomposite: An optical sensor for ammonia detection. *International Journal of Biological Macromolecules*, *51*, 583–589.

Pandey, S., Goswami, G. K., & Nanda, K. K. (2013a). Green synthesis of polysaccharide/gold nanoparticle nanocomposite: An efficient ammonia sensor. *Carbohydrate Polymers*, *94*, 229–234.

Pandey, S., Goswami, G. K., & Nanda, K. K. (2013b). Nanocomposite based flexible ultrasensitive resistive gas sensor for chemical reactions studies. *Scientific Reports*, *3*, 2082.

Pradhan, N., Pal, A., & Pal, T. (2002). Silver nanoparticle catalyzed reduction of aromatic nitro compounds. *Colloids and Surfaces A: Physicochemical and Engineering Aspects*, *196*, 247–257.

Qiu, L., Peng, Y., Liu, B., Lin, B., Peng, Y., Malik, M. J., & Yan, F. (2012). Polypyrrole nanotube-supported gold nanoparticles: An efficient electrocatalyst for oxygen reduction and catalytic reduction of 4-nitrophenol. *Applied Catalysis A: General*, *413-414*, 230–237.

Rakap, M., & Özkar, S. (2012). Hydroxyapatite-supported cobalt(0) nanoclusters as efficient and cost-effective catalyst for hydrogen generation from the hydrolysis of both sodium borohydride and ammonia–borane. *Catalysis Today*, *183*, 17–25.

Reiss, H. (1951). The growth of uniform colloidal dispersions. *Journal of Chemical Physics*, *19*, 482.

Sen, I. K., Maity, K., & Islam, S. S. (2013). Green synthesis of gold nanoparticles using a glucan of an edible mushroom and study of catalytic activity. *Carbohydrate Polymers*, *91*, 518–528.

Shah, M. A. (2012). Growth of uniform nanoparticles of platinum by an economical approach at relatively low temperature. *Scientia Iranica*, *19*, 964–966.

Shin, K. S., Choi, J.-Y., Park, C. S., Jang, H. J., & Kim, K. (2009). Facile synthesis and catalytic application of silver-deposited magnetic nanoparticles. *Catalysis Letters*, *133*, 1–7.

Tian, B., Zhang, J., Tong, T., & Chen, F. (2008). Preparation of $Au/TiO_2$ catalysts from Au(I)–thiosulfate complex and study of their photocatalytic activity for the degradation of methyl orange. *Applied Catalysis B: Environmental*, *79*, 394–401.

Tongsakul, D., Nishimura, S., Thammacharoen, C., Ekgasit, S., & Ebitani, K. (2012). Hydrotalcite-supported platinum nanoparticles prepared by a green synthesis method for selective oxidation of glycerol in water using molecular oxygen. *Industrial and Engineering Chemistry Research*, *51*, 16182–16187.

U.S. Department of Health and Human Services (USDHHS), & Hazardous Substances Data Bank. (1993). *National toxicology information program*. Bethesda, MD: National Library of Medicine.

Vinod, V. T. P., Saravanan, P., Sreedhar, B., Devi, D. K., & Sashidhar, R. B. (2011). A facile synthesis and characterization of Ag, Au and Pt nanoparticles using a natural hydrocolloid gum kondagogu (*Cochlospermum gossypium*). *Colloids and Surfaces B: Biointerfaces*, *83*, 291–298.

Xu, W., Jin, W., Lin, L., Zhang, C., Li, Z., Li, Y., Song, R., & Li, B. (2014). Green synthesis of xanthan conformation-based silver nanoparticles: Antibacterial and catalytic application. *Carbohydrate Polymers*, *101*, 961–967.

Xue, Y. P., Lu, X. F., Bian, X. J., Lei, J. Y., & Wang, C. (2012). Facile synthesis of highly dispersed palladium/polypyrrole nanocapsules for catalytic reduction of *p*-nitrophenol. *Journal of Colloid and Interface Science*, *379*, 89–93.

Zhang, W., Tan, F., Wang, W., Qiu, X., Qiao, X., & Chen, J. (2012). Facile, template-free synthesis of silver nanodendrites with high catalytic activity for the reduction of *p*-nitrophenol. *Journal of Hazardous materials*, *217–218*, 36–42.